ADVANCES IN ATMOSPHERIC SCIENCES, VOL. 37, MARCH 2020, 259–268

• **Original Paper** •

Contributions to the Interannual Summer Rainfall Variability in the Mountainous Area of Central China and Their Decadal Changes

Kaiming HU[*1,2,3], Yingxue LIU[2,4], Gang HUANG[2,3,5], Zhuoqi HE[6,2], and Shang-Min LONG[7,6]

[1]*Center for Monsoon System Research*, *Institute of Atmospheric Physics*, *Chinese Academy of Sciences*, *Beijing* 100029, *China*
[2]*State key Laboratory of Numerical Modeling for Atmospheric Sciences and Geophysical Fluid Dynamics*, *Institute of Atmospheric Physics*, *Chinese Academy of Sciences*, *Beijing* 100029, *China*
[3]*Joint Center for Global Change Studies (JCGCS)*, *Beijing* 100875, *China*
[4]*University of Chinese Academy of Sciences*, *Beijing* 100049, *China*
[5]*Laboratory for Regional Oceanography and Numerical Modeling*, *Qingdao National Laboratory for Marine Science and Technology*, *Qingdao* 266237, *China*
[6]*State Key Laboratory of Tropical Oceanography*, *South China Sea Institute of Oceanology*, *Chinese Academy of Sciences*, *Guangzhou* 510301, *China*
[7]*College of Oceanography*, *Hohai University*, *Nanjing* 210098, *China*

(Received 5 May 2019; revised 26 October 2019; accepted 18 November 2019)

ABSTRACT

Using a high-resolution precipitation dataset, the present study detected that the mountainous area of central China (MACA) is a hotspot of ENSO's impact on the summer rainfall variability. Further analysis suggests that both ENSO and atmospheric forcing make contributions to the summer rainfall variability in MACA. The dominant rainfall-related SST mode features as a seasonal transition from an El Niño-like warming in the preceding winter to a La Nina-like cooling in the following autumn, and it explains about 29% of the total variance of the rainfall during 1951–2018. It indicates that ENSO with a rapid phase transition is responsible for inducing summer rainfall anomalies in MACA. Besides, an upper-level circumglobal wave mode in the Northern Hemisphere during summer also explains about 29% of the summer rainfall variance. Contributions of both the SST and the atmospheric modes have experienced interdecadal changes. The influence of the SST mode gradually increases and plays a dominant role in the recent decades, suggesting that ENSO with a rapid phase transition becomes more important for rainfall prediction in MACA.

Key words: summer rainfall, ENSO, atmospheric internal variability, interdecadal change

Citation: Hu, K. M., Y. X. Liu, G. Huang, Z. Q. He, and S.-M. Long, 2020: Contributions to the interannual summer rainfall variability in the mountainous area of central China and their decadal changes. *Adv. Atmos. Sci.*, **37**(3), 259–268, https://doi.org/10.1007/s00376-019-9099-5.

Article Highlights:

- MACA is a hotspot of ENSO's impact on the summer rainfall variability.
- ENSO with a rapid phase transition becomes more important for summer rainfall variability in MACA.

1. Introduction

Summer (June–August) is the major rainy season for East Asia (Tao and Chen, 1987). Rainfall variability during summer is of great socioeconomic importance for China. Central China (box in Fig. 1a) has a special mountainous location. It includes the two largest rivers of China—the Yellow and the Yangtze—and has a population of more than 100 million. Heavy rainfall over such steep mountainous regions can cause landslides and floods, bringing huge damage to the local and downstream residents. Hence, it is important to understand the causes of the year-to-year variations of summer rainfall over the mountainous area of central China (MACA).

ENSO is widely considered as an important factor for

* Corresponding author: Kaiming HU
Email: hkm@mail.iap.ac.cn

China's summer rainfall (Fu and Ye, 1988; Huang and Wu, 1989; Shen and Lau, 1995; Chang et al., 2000; Wang et al., 2000; Wu et al., 2003, 2009, 2010; Xie et al., 2009; Ye and Lu, 2011; Kosaka et al., 2013; He and Wu, 2014; Zhang et al., 2016; He et al., 2017; Li et al., 2017). A low-level anomalous anticyclone over the tropical Northwest Pacific often develops in the El Niño mature phase and persists into the following summer (Zhang et al., 1996; Wang et al., 2000; Yang et al., 2007; Li et al., 2008; Xie et al., 2009; Stuecker et al., 2013). The anomalous anticyclone strengthens the northward vapor transport from the tropics to China, and is considered to be an important source of predictability for Chinese summer rainfall (Kosaka et al., 2013; Wang et al., 2013).

Using a newly released high-resolution dataset from 1979 to 2014, Hu et al. (2017) detected that a considerable number of stations in MACA show positive correlations of summer rainfall with the preceding winter Niño3 index during 1979–2014. They argued that ENSO could anchor its influence on the summer rainfall anomaly pattern in MACA via the orographic effects associated with anomalous atmospheric circulation. In central China, there are several east–west-oriented mountain ranges, including the Wushan, Bashan and Qinling Mountains and the Loess Plateau. In the post-El Niño summer, anomalous Northwest Pacific anticyclones intensify the moisture advection from the tropics, causing increased rainfall when arriving at these mountain ranges.

However, there are still some key issues to be addressed. Previous studies have implied that teleconnection between ENSO and remote areas is not always stable. For example, ENSO's impact on the Northwest Pacific summer monsoon strengthens after the mid-1970s (Wang et al., 2008; Huang et al., 2010; Xie et al., 2010), and its relationship with the Indian Ocean SSTs and the Indian summer monsoon weakens in recent decades (Kumar et al., 2006; He and Wu, 2018). In addition, the midlatitude atmospheric internal modes, such as the low-frequency wave train, are as important factors as ENSO for the East Asian climate variability (Lu et al., 2002; Ding and Wang, 2005; Kosaka et al., 2009; Li and Sun., 2015; Hu et al., 2018). Does the relationship between ENSO and summer rainfall in central China experience significant interdecadal changes? If so, are there any other factors affecting the interannual variability of summer rainfall in MACA? These questions remain to be answered.

This study aims to address the above questions to gain insight into the mechanism of MACA summer rainfall variations. Firstly, we diagnose whether the relationship between ENSO and summer rainfall in MACA is stable in the period 1951–2018. Then, we investigate the principal sea surface temperature (SST) and the atmospheric modes related to the summer rainfall variability in MACA, and finally estimate the relative contributions of each factor.

2. Data

Two observed rainfall datasets are used in this study. One is a newly released high-resolution precipitation dataset containing 2400 observation stations in China. The earliest record goes back to 1 January 1951 and updates to 31 December 2014. The number of available stations increases gradually from 165 in 1951 to 2298 in 1979. After 1979, the spatial resolution is high enough to capture the orographic effect on rainfall. The other is a relative coarse-resolution precipitation dataset that contains 75 observation stations in China from 1 January 1951 to 31 December 2018. Both of these two sets of observed rainfall data are obtained from the China Meteorological Data Service Center (http://data.cma.cn/en). The first dataset has a higher spatial resolution, while the second has a longer record. As shown in section 3, the interannual variabilities of area-mean MACA summer rainfall derived from the two datasets are highly consistent during 1979–2014. Thus, we use the 1979–2014 high-resolution dataset to identify the ENSO-related rainfall pattern in China, while we use the 1951–2018 coarse-resolution dataset to check whether ENSO influences summer rainfall in China steadily. The monthly mean winds and water vapor fluxes are derived from the 2.5° latitude × 2.5° longitude monthly NCEP-1 reanalysis data (Kalnay et al., 1996) provided by the NOAA/OAR/ESRL PSD, Boulder, Colorado, USA (https://www.esrl.noaa.gov/psd/). The monthly SST data are from the global gridded monthly SST dataset from the UK Met Office Hadley Centre (Rayner et al., 2003), which has the resolution of 1° × 1° and is available since 1870. Statistical significance in this study is evaluated by the two-sided Student's *t*-test.

3. Results

3.1. *ENSO's impact on MACA summer rainfall*

Figure 1a shows the stations with significant correlation between the June–August (JJA) mean rainfall and the preceding November–January [NDJ(0)] mean Niño3 (5°S–5°N, 90°–150°W) SST index during 1979–2014 based on the high-resolution dataset. Most stations with significant positive correlation above the 95% confidence level are located in MACA. The MACA summer rainfall anomalies should be partly caused by the ENSO-induced anomalous anticyclone from the Bay of Bengal to the Northwest Pacific, as it intensifies southwesterly vapor flux from the tropics to MACA and causes vapor convergence in the mountainous area (Hu et al., 2017). For convenience, we use a rectangular area of (28°–37°N, 103°–113°E) (shown in Fig. 1a) to represent MACA. In this area, 126 out of 430 stations show positive correlations above the 95% confidence level. It is clear that the JJA rainfall anomaly in MACA closely coincides with the NDJ(0) Niño3 SST anomaly, with the correlation reaching as high as 0.54 (above the 99% confidence level) (Fig. 1b). The evidence indicates that the summer rainfall in MACA is closely related to ENSO during 1979–2014.

However, the relatively short record of the high-resolution rainfall dataset limits us to understand whether or not this ENSO–rainfall relationship has interdecadal changes.

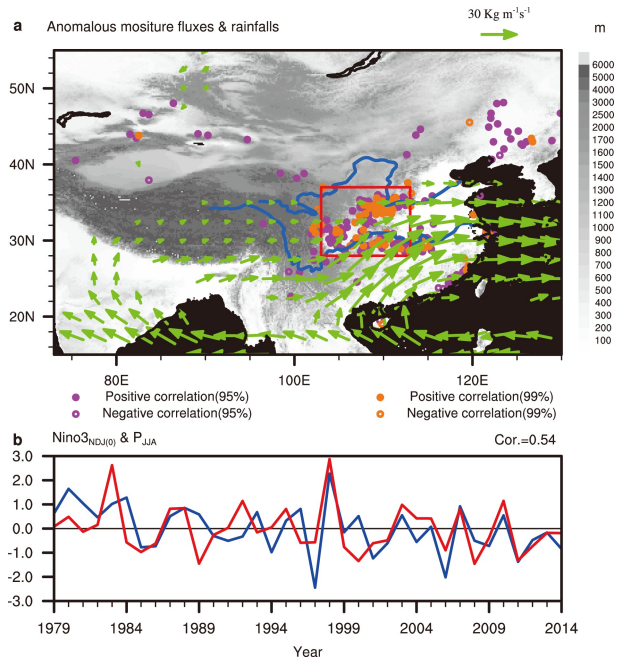

Fig. 1. (a) Stations (dots) with significant correlations between the JJA rainfall and the preceding NDJ(0) Niño3 SST index, and regressions (vectors; units: kg m^{-1} s^{-1}) of the vertically integrated (from surface to 200 hPa) moisture flux with the NDJ(0) Niño3 SST index during 1979–2014. (b) Normalized JJA rainfall (blue line) averaged in the rectangular box in (a) and the NDJ(0) Niño3 SST index (red line). The gray shading in (a) denotes the topography (units: m). The magenta and the orange solid (hollow) dots represent positive (negative) correlations exceeding the 95% and the 99% confidence levels, respectively. Only flux anomalies that are significant at the 90% confidence level are plotted. The rectangular area denotes MACA.

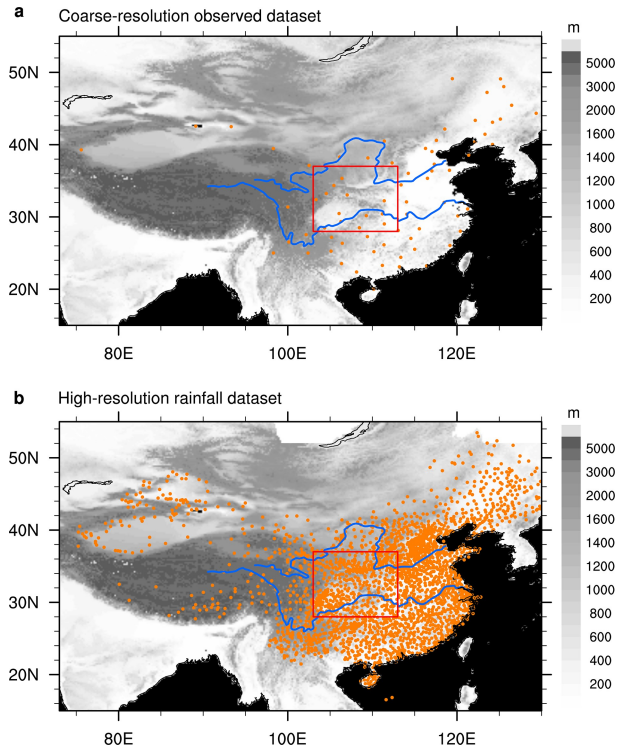

Fig. 2. The distribution of stations (orange dots) in the coarse-resolution observed dataset with 74 stations (a) and in the high-resolution rainfall dataset (b), superimposed on elevation (gray shading; units: m). Blue lines mark the Yellow and Yangtze rivers. The rectangular area denotes MACA.

Here, another rainfall dataset with a coarse resolution that has a longer record from 1951 to 2018 is used, which contains 12 stations in the rectangular area of (28°–37°N, 103°–113°E). The distributions of stations in the two datasets are shown in Fig. 2. The 12-station-averaged JJA rainfall anomaly during 1951–2018 is shown in Fig. 3a, denoted as *P* index. The correlation of *P* index and the area-mean JJA rainfall anomaly based on the high-resolution dataset during 1979–2014 is as high as 0.87 (Fig. 2a), above the 99% confidence level. Thus, the *P* rainfall index is considered as a good proxy to represent the summer rainfall variability in MACA. To examine the evolution of the ENSO–rainfall relationship in a longer period, Fig. 3b shows the correlation in a 21-year sliding window between the NDJ(0) Niño3 SST index and the *P* rainfall index from 1951 to 2018. It is evident that the 21-year sliding correlation is weak (−0.1 to 0.3) before the mid-1970s and during the period of 1982–88, and it is significant at the 90% confidence level in most other periods. Here, another feature to be noted is that the correlation coefficient rises rapidly after the 2000s and it reaches up to 0.64 in 2008. The result denotes that the relationship between ENSO and the summer rainfall in MACA has experienced significant interdecadal changes.

We further select two periods, 1951–79 and 1990–2018, to document the interdecadal change. The correlation coefficients between *P* index and the NDJ(0) Niño3 SST index during the two periods are 0.10 and 0.54, respectively. Figures 3c and d present the regression of JJA wind velocity at 850 hPa onto the NDJ(0) Niño3 SST index for 1951–79 and 1990–2018. Notable differences can be found between these two periods. During 1990–2008, the lower-level wind anomaly forms a dipole pattern over the Indian Ocean–western Pacific. A strong cyclonic anomaly develops along the tropical Maritime Continent and the Indian Ocean, and a significant anticyclonic anomaly extends from the subtropical Northwest Pacific to China. In this case, the anomalous anticyclone over the Northwest Pacific favors moisture transport from the tropics to MACA and causes increased rainfall via the orographic lifting effect (Hu et al., 2017). In contrast, the ENSO-related anomalous anticyclone over the Northwest Pacific is much weaker and locates far to the east during 1951–79. Consequently, the impact of ENSO on the summer rainfall in MACA is weaker in the pre-period than the post-period. The result is consistent with previous studies pointing out that ENSO's impact on the Northwest Pacific anticyclone strengthens in the recent decades (Wang et al., 2008; Huang et al., 2010; Xie et al., 2010).

3.2. *Principal modes for the summer rainfall variability*

As shown in Fig 3a, ENSO's teleconnection with the summer rainfall variability in MACA features significant in-

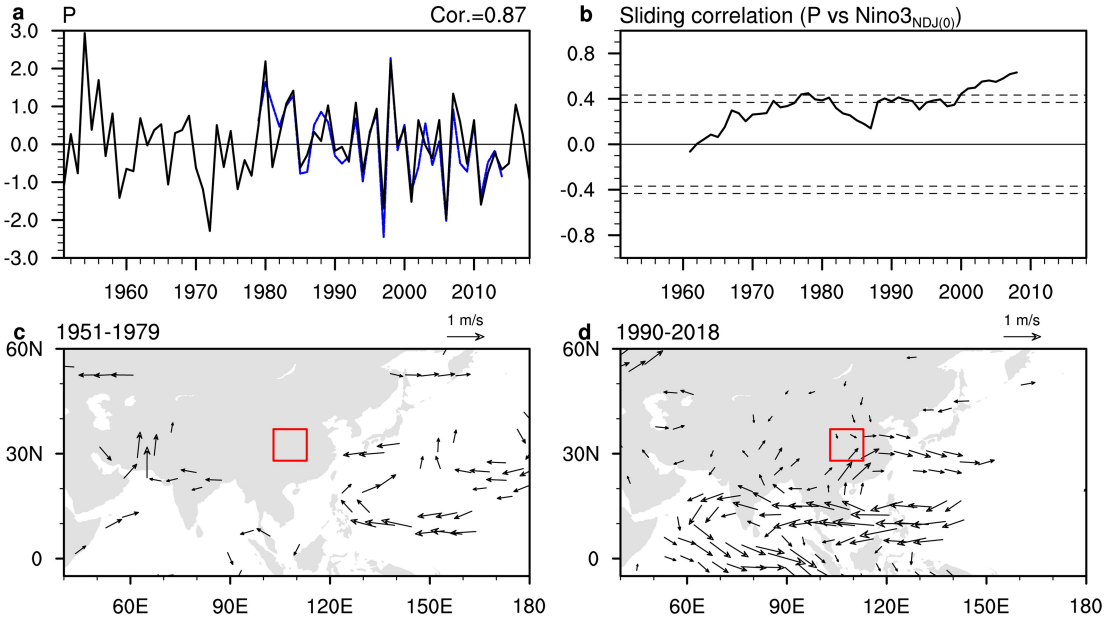

Fig. 3. (a) Normalized JJA rainfall anomalies averaged in the rectangular box of MACA derived from the coarse-resolution (black line) and the high-resolution (blue line) precipitation datasets, and their correlation is 0.87 during 1979–2014. (b) The 21-year sliding correlation between the normalized JJA rainfall anomaly averaged in the rectangular box derived from the coarse-resolution precipitation dataset and the NDJ(0) Niño3 SST index during 1951–2018, and the dotted horizontal lines denote the 95% and 99% confidence levels respectively. (c) Regressions (vectors; units: m s^{-1}) of JJA mean winds at 850 hPa onto the NDJ(0) Niño3 SST index during 1951–79. (d) Regressions (vectors; units: m s^{-1}) of JJA mean winds at 850 hPa onto the NDJ(0) Niño3 SST index 1990–2018. The rectangular area in (c) and (d) denotes MACA. Only wind anomalies that are significant at the 90% confidence level are plotted.

terdecadal changes. This implies that the summer rainfall anomalies may also be governed by other factors. In this subsection, a statistical method called partial least-squares (PLS) regression (Abdi, 2010) is employed to identify the principal factors for the rainfall variability in MACA. PLS regression has been widely used to identify factors for East Asian climate variations (Wu and Yu, 2016).

Evidence shows that East Asian summer climate is not only affected by the amplitude of the SST modes but also by the decaying or developing paces of them (Chen et al., 2016b; Jiang et al., 2017). To obtain the seasonally evolving principal SST patterns associated with the JJA rainfall variability in MACA, we conduct PLS regression by the following procedure. First, we construct a predictor array $X(t, j, k)$ of year-to-year variations in four consecutive seasons' tropical SST (30°S–30°N) from the preceding winter DJF(0) to the following autumn (September–November, SON), where t, j and k respectively denote the years (from 1951 to 2018), the four consecutive seasons, and the grid point in the tropics. Then, the array $X(t, j, k)$ is regressed onto the normalized P rainfall index to obtain a regression map $Z(j, k)$. Here, the SST fields in the four consecutive seasons are treated as an integral block in the regression analysis. After the regression, the yearly block is divided into four consecutive seasonal SST anomalies, so that the regression map $Z(j, k)$ contains a set of seasonally evolving patterns of SST anomalies from DJF(0) to SON. The regression map $Z(j, k)$ is the first leading SST mode associated with the P rainfall index. Second, we project the array $X(t, j, k)$ onto the $Z(j, k)$ to obtain a score array $\mathrm{PSL}_{\mathrm{SST}}(t)$ using the pattern regression method. The score array $\mathrm{PSL}_{\mathrm{SST}}(t)$ is the time series of the first leading SST mode. The part of the P rainfall index linearly related to $\mathrm{PSL}_{\mathrm{SST}}(t)$ is considered as the component contributed by the SST mode. Third, the $\mathrm{PSL}_{\mathrm{SST}}(t)$ is regressed out of both in the array $X(t, j, k)$ and the P rainfall index to obtain residual arrays $X_{\mathrm{r}}(t, j, k)$ and P_{r}. The above three steps are repeated using the residual arrays $X_{\mathrm{r}}(t, j, k)$ and P_{r} until the successive SST modes no longer explain a sizeable fraction of the variance of the rainfall. This procedure is similar to that used by Wallace et al. (2012).

The first SST mode $Z(j, k)$ features an El Niño-like pattern in the preceding winter (Fig. 4a). This pattern weakens in spring, turns negative in the central equatorial Pacific in summer, and transitions to a La Nina-like pattern in the following autumn, which explains about 29% of the total variance of the P rainfall index during 1951–2018. Accompanied by the SST mode, there are prominent anticyclonic anomalies at 850 hPa from the Northwest Pacific to China in summer, which is likely a key bridge to link the SST mode with the summer rainfall in central China. The correlation coefficient of the P rainfall index with the time series of the first SST mode is 0.54 (above the 99% confidence level) during 1951–2018, which is much higher than the correlation (r = 0.33) with the NDJ(0) Niño3 SST index. The result suggests that ENSO events with rapid phase transition tend to have a tighter relationship with MACA summer rainfall,

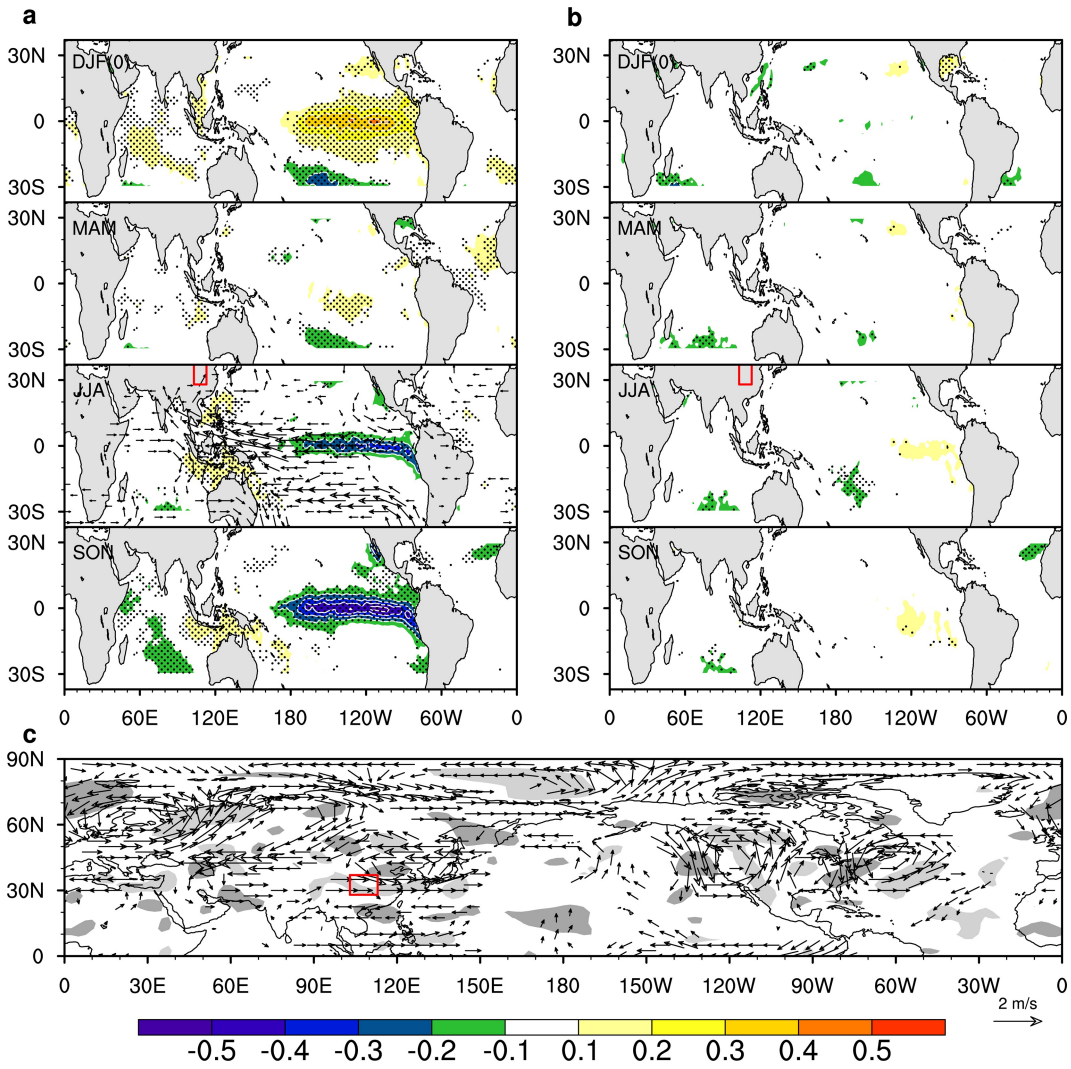

Fig. 4. Seasonally varying SST anomalies (color shading; dotted areas pass the 95% confidence level; units: K) from the preceding winter [DJF(0)] to the following autumn (SON) in the first (a) and the second (b) leading SST PLS regression modes. The vectors in (a) are the regressions of JJA mean winds at 850 hPa onto the time series of the first leading SST PLS regression modes during 1951–2018. (c) Regression of 200 hPa JJA wind (vectors; only those exceeding the 90% confidence level are shown) and the correlation of the 500-hPa JJA omega field (gray shading) with the time series of the first leading v200 PLS regression mode (PSL_{v200}) during 1951–2018. The dark (light) gray shading in (c) represents positive (negative) correlations above the 90% confidence level. The method of PLS regression is described in section 3.

likely because summer equatorial Pacific cooling strengthens the lower-level anomalous anticyclone in the Northwest Pacific (Xiang et al., 2013; Chen et al., 2016a; Fan et al., 2016; Jiang et al., 2017). Moreover, anomalous warm SST in the northern tropical Atlantic region are found in the boreal spring (Fig. 4a), which could trigger a La Niña event in the following winter (Ham et al., 2013; Wang et al., 2017), thus leading to the rapid phase transition from El Niño to La Niña. The SST anomalies in the second SST mode (Fig. 4b) are very weak and insignificant in all four seasons, and the variance of rainfall explained by the second SST mode is relatively small (about 10.6%). The variance of rainfall explained by other SST modes (not shown) is negligible.

The first two SST modes explain only about 39.6% of the total variance of the P rainfall index during 1951–2018, leaving a large fraction of unexplained variance. Observational evidence shows that low-frequency wave activities in the midlatitudes are another important source for East Asian summer climate variability (Lu et al., 2002; Ding and Wang, 2005; Kosaka et al., 2009). We thus further look for the principal atmospheric modes associated with the residual rainfall variability via PLS regression. The procedure is similar to that used to detect the SST modes. However, here, the predictor array $X(t,k)$ refers to the yearly varying JJA-mean meridional wind v at 200 hPa in the Northern Hemisphere from 1951 to 2018, and the predictand time series is the residual rainfall index P_r, with the first leading SST mode contributions having been removed, where t and k respectively denote the years during 1951–2018 and the grid points in the

Northern Hemisphere (0°–90°N). We utilize the *v* field as the predictor array because it would preferentially emphasize the wave trains (Branstator, 2002). Following the procedure, we calculate the first two leading modes of *v* and their corresponding time series $PSL1_{v200}$ and $PSL2_{v200}$. The correlations of *P* rainfall index with $PSL1_{v200}$ and $PSL2_{v200}$ are 0.54 and 0.35, respectively. So, the first and second leading *v* modes can explain 29% and 12% of the total variance in the *P* rainfall index. In this study, we mainly focus on the first leading *v* modes.

The regression (Fig. 4c) of JJA 200-hPa winds onto the $PSL1_{v200}$ features as a circumglobal wave train structure, with cyclonic centers in Europe, the Middle East, East Asia, the west and east coast of North America, and anticyclonic centers over Kazakhstan, the central North Pacific and North America. Around MACA, there are significant anomalous westerly winds along the latitude of around 30°N from 90°E to 150°E, which may intensify warm advection from the climatological temperature maximum over the Tibetan Plateau, inducing additional upward motion (gray shading in Fig. 4c) in favor of increased rainfall in central China (Sampe and Xie, 2010; Hu et al., 2017). For convenience, this regression map is denoted as the first leading atmospheric mode. The correlation of $PSL1_{v200}$ with $PSL1_{SST}$ is near zero, indicating the impacts from the first SST and the first atmospheric modes on MACA summer rainfall change are mutually orthogonal. The correlation of $PSL1_{v200}$ with the *P* rainfall index is 0.54 (above the 99% confidence level) during 1951–2018, suggesting that the first atmospheric mode explains about 29% of the total rainfall variance.

3.3. *Relative role of the SST and atmospheric modes*

To quantitively evaluate the relative role of the two dominant modes in explaining the MACA summer rainfall variability, we calculate the component of rainfall change from these two modes. The component of rainfall linearly related to the first leading SST mode (Fig. 5a) is denoted by $PSL1_{SST}$×0.54. Here, $PSL1_{SST}$ is the normalized time series

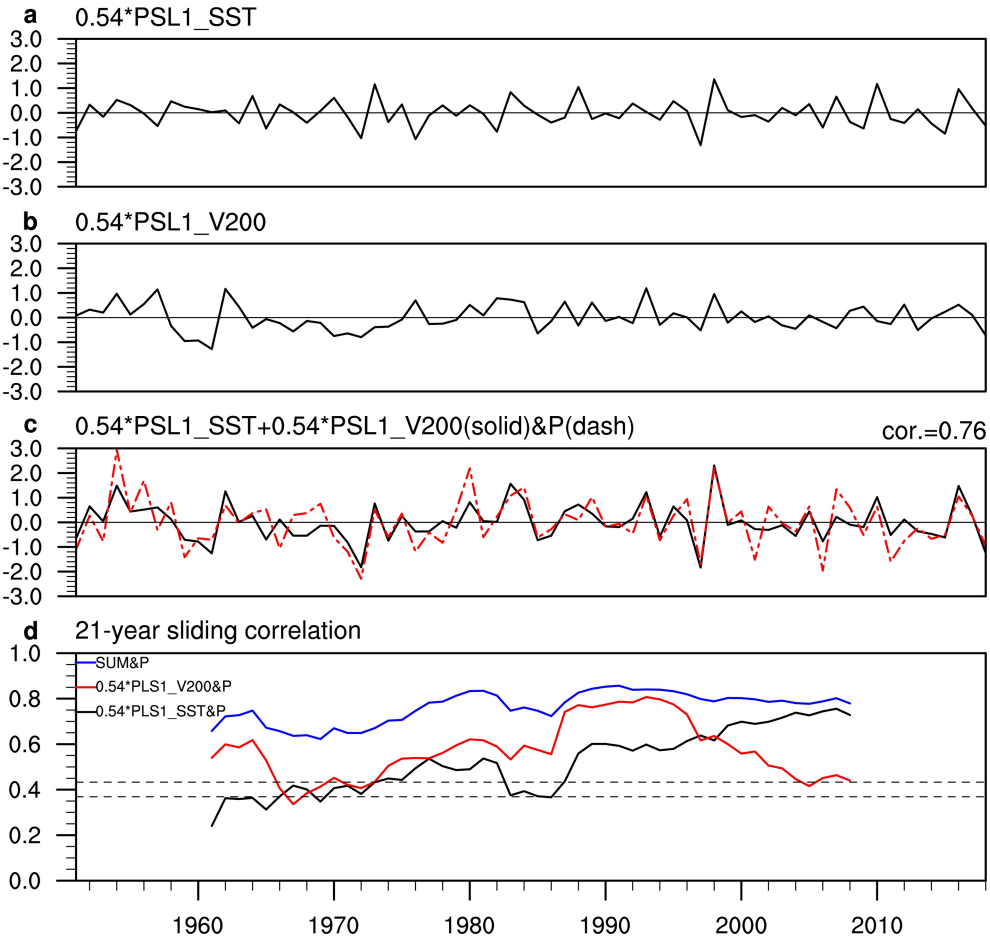

Fig. 5. Component of rainfall linearly related to the (a) first SST PLS regression modes ($PSL1_{SST}$×0.54) and (b) first leading v200 PLS regression mode ($PSL1_{v200}$×0.54). (c) Normalized *P* summer rainfall index (red dashed line) and the sum (black solid line) of $PSL1_{v200}$×0.54 and $PSL1_{SST}$×0.54. (d) 21-year sliding correlation of the *P* summer rainfall index with $PSL1_{SST}$×0.54 (black line), $PSL1_{v200}$×0.54 (red line) and $PSL1_{SST}$×0.54+$PSL1_{v200}$×0.54 (blue line) during 1951–2018, where the dotted horizontal lines denote the 95% and 99% confidence levels, respectively.

of the SST mode and 0.54 is the regression coefficient of the rainfall index P onto the $PSL1_{SST}$. Similarly, the linear component of rainfall related to the first leading atmospheric mode (Fig. 5b) is denoted by $PSL1_{v200}\times0.54$, and $PSL1_{v200}$ is the normalized time series of the atmospheric mode and 0.54 is the regression value of the residual rainfall index P_r onto the $PSL1_{v200}$. The contribution of the SST mode and the atmospheric mode are independent of each other because $PSL1_{SST}$ and $PSL1_{v200}$ are mutually orthogonal during 1951–2015. The two modes both explain about 29% of the total rainfall variance during 1951–2018, suggesting their influences on summer rainfall in MACA is of equal importance. However, their influences in MACA summer rainfall change are noticeable in different years. For example, the rainfall anomalies in the years of 1959, 1960, 1961, 1961, 1989 and 1993 are mainly contributed by the atmospheric mode, while the rainfall anomalies in the years of 1997, 1998, 2007, 2010 and 2016 are largely due to the SST mode. The total contribution of the first SST mode and the atmospheric mode is denoted by $PSL_{sum}= PSL1_{SST}\times0.54+ PSL1_{v200}\times0.54$ (Fig. 5c). The combined index PSL_{sum} is highly correlated with the rainfall index P, with the correlation coefficient up to 0.76 (above the 99% confidence level) during 1951–2018. Therefore, the two modes together can explain most year-to-year variance of MACA summer rainfall.

Figure 5d shows the 21-year sliding correlation of $PSL1_{SST}\times0.54$, $PSL1_{v200}\times0.54$ and PSL_{sum} with the rainfall index P during 1951–2018. The correlation (black line) between $PSL1_{SST}\times0.54$ and the P rainfall index is above the 90% confidence level in most periods, especially after the mid-1960s. After 1986, it rises dramatically and reaches to 0.75 in 2008. Similarly, the 21-year sliding correlation (red line) between $PSL1_{v200}\times0.54$ and the rainfall index P also exceeds the 90% confidence level in most periods. However, it peaks around the early 1960s and the 1990s, and decreases dramatically after the late 1990s. The result shows that both the SST mode and the atmospheric mode influences on summer rainfall in MACA display substantial interdecadal change during 1951–2018. It is worth noting that in the recent decades the influence from the SST mode on summer rainfall in MACA increases while the role of the atmospheric mode decreases, suggesting evolved roles of the SST and atmospheric modes over time. The 21-year sliding correlation of the P rainfall index (black line) with the combined index PSL_sum ranges from 0.62 to 0.86 through the whole period, which is higher and more stable than that with $PSL1_{SST}\times0.54$ and $PSL1_{SST}\times0.54$ alone. In addition, we calculate the sliding correlations of $PSL1_{SST}$ and $PSL1_{v200}$ with the NDJ(0) Niño3.4 SST index during 1951–2018 (Fig. 6). The relationship between the NDJ(0) Niño3.4 SST index and the SST mode is tight and stable during 1951–2018, with the 21-year sliding correlations above 0.6 in most periods. Consequently, the interdecadal changes in ENSO's impact on MACA summer rainfall are consistent with the interdecadal changes in the relationship between rainfall and the SST mode. The relationship between the NDJ(0) Niño3.4 SST index and the atmospheric mode is weak, suggesting their impacts on MACA summer rainfall are generally independent of each other.

4. Summary and discussion

Using a high-resolution precipitation dataset, the present study detected that the summer rainfall variability over MACA is highly related to ENSO. Further, based on a coarse-resolution rainfall dataset with a longer time period, we found that the relationship between the NDJ(0) Niño3 SST index and the summer rainfall anomaly in MACA experiences interdecadal changes, weakened in the 1950s and 1960s and strengthened after the late 1980s. Changes in the ENSO–rainfall relationship are likely attributable to the enhancement of ENSO's impact on the summer Northwest Pacific anticyclone in the recent decades (Wang et al., 2008; Huang et al., 2010; Xie et al., 2010). After the mid-1980s, the anomalous anticyclone over the subtropical Northwest Pacific in the post-El Niño summer turns to be stronger and extends further west, compared with that in the 1950s, 1960s and 1970s. This results in enhanced vapor transport from the tropics to MACA. Consequently, the summer rainfall variability in MACA is more closely related to ENSO forcing after the mid-1980s.

According to the PLS regression analysis, we identi-

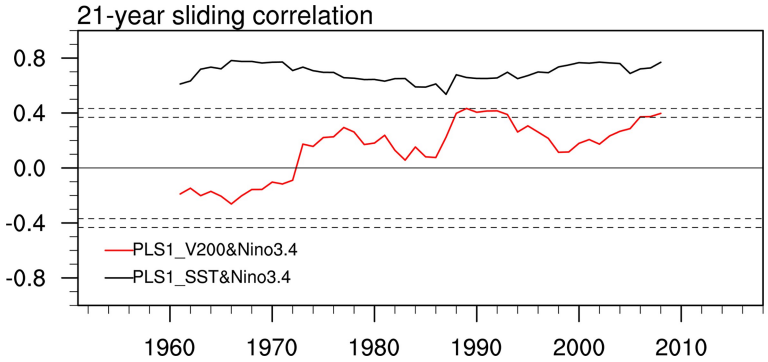

Fig. 6. 21-year sliding correlation of the NDJ(0) Niño3 SST index with $PSL1_{SST}$ (black line) and $PSL1_{v200}$ (red line) during 1951–2018. The dotted horizontal lines denote the 95% and 99% confidence levels, respectively.

fied the dominant SST and atmospheric circulation modes that contribute to the JJA rainfall variability in MACA. The SST mode features as a seasonal transition from an El Niño-like warming in the preceding winter to a La Nina-like cooling in the following autumn. The time series of the first SST mode presents a higher correlation with the *P* rainfall index than the NDJ(0) Niño3 SST index. It signifies that the summer rainfall variability in MACA is mainly contributed by ENSO events with a rapid phase transition. ENSO's seasonal phase transitions should be considered for the rainfall prediction in MACA. The atmospheric circulation mode features as a circumglobal wave train structure in the Northern Hemisphere. The contributions of the first SST mode and the first atmospheric mode are mutually independent, and they explain the majority of the rainfall variance with a contribution of 29%, respectively.

Both the contributions of the SST mode and the atmospheric mode have experienced interdecadal change during 1951–2018. The 21-year sliding correlation of the JJA rainfall index with the time series of the first SST mode generally rises gradually from 0.25 in 1961 to 0.75 in 2008, and the correlation with the time series of the first atmospheric mode peaks around the 1990s and declines afterward. The result suggests that the influence of the SST mode on the summer rainfall anomaly in MACA is strengthened, while the influence of the atmospheric mode decreases during recent decades. There may be some possible reasons for the interdecadal changes. First, ENSO amplitudes enhance after the late 1970s, so the relation between eastern Pacific SST and the summer monsoonal circulation over the East Asian–Northwest Pacific region becomes tighter (Wang et al., 2008). Second, the interdecadal change is partly due to changes in the tropical Indian Ocean (TIO) response to ENSO (Huang et al., 2010; Xie et al., 2010). After the late 1970s, the El Niño-induced TIO warming persists larger than that before. Third, the decadal change may be partly due to the rise of influences from the Atlantic Ocean SST during recent decades (Yu et al., 2015; Wang et al., 2017; Wang and Yu, 2018). Given the increasing importance of ENSO's role since the recent decades, monitoring ENSO's amplitude and its phase transition may help summer rainfall prediction in MACA.

Acknowledgements. This study was jointly supported by the National Key R&D Program of China (2019YFA0606703), the Strategic Priority Research Program of Chinese Academy of Sciences (XDA20060502), the Strategic Priority Research Program of Chinese Academy of Sciences (Grant No. XDA20060502), the National Natural Science Foundation of China (Grant Nos. 41425086, 41661144016, 41706026, 41506003 and 41731173), and the State Key Laboratory of Tropical Oceanography, South China Sea Institute of Oceanology, Chinese Academy of Sciences (Project No. LTO 1704). The authors declare no competing interests.

REFERENCES

Abdi, H., 2010: Partial least squares regression and projection on latent structure regression (PLS Regression). *Wiley Interdisciplinary Reviews*: *Computational Statistics*, **2**, 97–106, https://doi.org/10.1002/wics.51.

Branstator, G., 2002: Circumglobal teleconnections, the jet stream waveguide, and the North Atlantic Oscillation. *J. Climate*, **15**, 1893–1910, https://doi.org/10.1175/1520-0442(2002)015<1893:CTTJSW>2.0.CO;2.

Chang, C.-P., Y. S. Zhang, and T. Li, 2000: Interannual and interdecadal variations of the East Asian summer monsoon and tropical Pacific SSTs. Part I: Roles of the subtropical ridge. *J. Climate*, **13**, 4310–4325, https://doi.org/10.1175/1520-0442(2000)013<4310:IAIVOT>2.0.CO;2.

Chen, W., J.-Y. Lee, K.-J. Ha, K.-S. Yun, and R. Y. Lu, 2016b: Intensification of the western north pacific anticyclone response to the short decaying El Niño event due to greenhouse warming. *J. Climate*, **29**, 3607–3627, https://doi.org/10.1175/JCLI-D-15-0195.1.

Chen, Z. S., Z. P. Wen, R. G. Wu, X. B. Lin, and J. B. Wang, 2016a: Relative importance of tropical SST anomalies in maintaining the Western North Pacific anomalous anticyclone during El Niño to La Niña transition years. *Climate Dyn.*, **46**, 1027–1041, https://doi.org/10.1007/s00382-015-2630-1.

Ding, Q. H., and B. Wang, 2005: Circumglobal teleconnection in the northern hemisphere summer. *J. Climate*, **18**, 3483–3505, https://doi.org/10.1175/JCLI3473.1.

Fan, L., S. I. Shin, Z. Y. Liu, and Q. Y. Liu, 2016: Sensitivity of Asian Summer Monsoon precipitation to tropical sea surface temperature anomalies. *Climate Dyn.*, **47**, 2501–2514, https://doi.org/10.1007/s00382-016-2978-x.

Fu, C. B., and D. Z. Ye, 1988: The tropical very low-frequency oscillation on interannual scale. *Adv. Atmos. Sci.*, **5**, 369–388, https://doi.org/10.1007/BF02656760.

Ham, Y.-G., J.-S. Kug, J.-Y. Park, and F.-F. Jin, 2013: Sea surface temperature in the north tropical Atlantic as a trigger for El Niño/Southern Oscillation events. *Nature Geoscience*, **6**, 112–116, https://doi.org/10.1038/ngeo1686.

He, C., A. L. Lin, D. J. Gu, C. H. Li, B. Zheng, and T. J. Zhou, 2017: Interannual variability of Eastern China Summer Rainfall: The origins of the meridional triple and dipole modes. *Climate Dyn.*, **48**, 683–696, https://doi.org/10.1007/s00382-016-3103-x.

He, Z. Q., and R. G. Wu, 2014: Indo-Pacific remote forcing in summer rainfall variability over the South China Sea. *Climate Dyn.*, **42**, 2323–2337, https://doi.org/10.1007/s00382-014-2123-7.

He, Z. Q., and R. G. Wu, 2018: Change in coherence of interannual variability of summer rainfall over the Western Pacific around the early 2000s: Role of Indo-Pacific ocean forcing. *J. Climate*, **31**, 3525–3538, https://doi.org/10.1175/JCLI-D-17-0687.1.

Hu, K. M., S.-P. Xie, and G. Huang, 2017: Orographically anchored El Niño effect on summer rainfall in central China. *J. Climate*, **30**, 10037–10045, https://doi.org/10.1175/JCLI-D-17-0312.1.

Hu, K. M., G. Huang, R. G. Wu, and L. Wang, 2018: Structure and dynamics of a wave train along the wintertime Asian jet and its impact on East Asian climate. *Climate Dyn.*, **51**, 4123–4137, https://doi.org/10.1007/s00382-017-3674-1.

Huang, G., K. M. Hu, and S.-P. Xie, 2010: Strengthening of tropical Indian ocean teleconnection to the Northwest Pacific since the mid-1970s: An atmospheric GCM study. *J. Climate*, **23**, 5294–5304, https://doi.org/10.1175/2010JCLI35

77.1.

Huang, R. H., and Y. F. Wu, 1989: The influence of ENSO on the summer climate change in China and its mechanism. *Adv. Atmos. Sci.*, **6**, 21–32, https://doi.org/10.1007/BF02656915.

Jiang, W. P., G. Huang, K. M. Hu, R. G. Wu, H. N. Gong, X. L. Chen, and W. C. Tao, 2017: Diverse relationship between ENSO and the Northwest Pacific summer climate among CMIP5 Models: Dependence on the ENSO decay pace. *J. Climate*, **30**, 109–127, https://doi.org/10.1175/JCLI-D-16-0365.1.

Kalnay, E., and Coauthors, 1996: The NCEP/NCAR 40-year reanalysis project. *Bull. Amer. Meteorol. Soc.*, **77**, 437–472, https://doi.org/10.1175/1520-0477(1996)077<0437:TNYRP>2.0.CO;2.

Kosaka, Y., H. Nakamura, M. Watanabe, and M. Kimoto, 2009: Analysis on the dynamics of a wave-like teleconnection pattern along the summertime asian jet based on a reanalysis dataset and climate model simulations. *J. Meteorol. Soc. Japan*, **87**, 561–580, https://doi.org/10.2151/jmsj.87.561.

Kosaka, Y., S.-P. Xie, N.-C. Lau, and G. A. Vecchi, 2013: Origin of seasonal predictability for summer climate over the Northwestern Pacific. *Proceedings of the National Academy of Sciences of the United States of America*, **110**, 7574–7579, https://doi.org/10.1073/pnas.1215582110.

Kumar, K. K., B. Rajagopalan, M. Hoerling, G. Bates, and M. Cane, 2006: Unraveling the mystery of indian monsoon failure during El Niño. *Science*, **314**, 115–119, https://doi.org/10.1126/science.1131152.

Li, C., and J. L. Sun, 2015: Role of the subtropical westerly jet waveguide in a southern China heavy rainstorm in December 2013. *Adv. Atmos. Sci.*, **32**, 601–612, https://doi.org/10.1007/s00376-014-4099-y.

Li, C. F., W. Chen, X. W. Hong, and R. Y. Lu, 2017: Why was the strengthening of rainfall in summer over the Yangtze River valley in 2016 less pronounced than that in 1998 under similar preceding El Niño events?—Role of midlatitude circulation in August *Adv. Atmos. Sci.*, **34**, 1290–1300, https://doi.org/10.1007/s00376-017-7003-8.

Li, S. L., J. Lu, G. Huang, and K. M. Hu, 2008: Tropical indian ocean basin warming and east Asian summer monsoon: A multiple AGCM study. *J. Climate*, **21**, 6080–6088, https://doi.org/10.1175/2008JCLI2433.1.

Lu, R.-Y., J.-H. Oh, and B. J. Kim, 2002: A teleconnection pattern in upper-level meridional wind over the North African and Eurasian continent in summer. *Tellus A*, **54**, 44–55, https://doi.org/10.3402/tellusa.v54i1.12122.

Rayner, N. A., D. E. Parker, E. B. Horton, C. K. Folland, L. V. Alexander, D. P. Rowell, E. C. Kent, and A. Kaplan, 2003: Global analyses of sea surface temperature, sea ice, and night marine air temperature since the late nineteenth century. *J. Geophys. Res.*, **108**, 4407, https://doi.org/10.1029/2002JD002670.

Sampe, T., and S.-P. Xie, 2010: Large-scale dynamics of the Meiyu-Baiu rainband: Environmental forcing by the westerly jet. *J. Climate*, **23**, 113–134, https://doi.org/10.1175/2009JCLI3128.1.

Shen, S., and K.-M. Lau, 1995: Biennial oscillation associated with the East Asian summer monsoon and tropical sea surface temperatures. *J. Meteorol. Soc. Japan*, **73**, 105–124, https://doi.org/10.2151/jmsj1965.73.1_105.

Stuecker, M. F., A. Timmermann, F. F. Jin, S. McGregor, and H.-L. Ren, 2013: A combination mode of the annual cycle and the El Niño/Southern Oscillation. *Nature Geoscience*, **6**, 540–544, https://doi.org/10.1038/ngeo1826.

Tao, S.-Y., and L. X. Chen, 1987: A review of recent research on the East Asian summer monsoon in China. *Monsoon Meteorology*, C.-P. Chan and T. N. Krishramuti, Eds., Oxford University Press, 60–92.

Wallace, J. M., Q. Fu, B. V. Smoliak, P. Lin, and C. M. Johanson, 2012: Simulated versus observed patterns of warming over the extratropical Northern Hemisphere continents during the cold season. *Proceedings of the National Academy of Sciences of the United States of America*, **109**, 14337–14342, https://doi.org/10.1073/pnas.1204875109.

Wang, B., R. G. Wu, and X. H. Fu, 2000: Pacific-East Asian teleconnection: How does ENSO affect East Asian climate? *J. Climate*, **13**, 1517–1536, https://doi.org/10.1175/1520-0442(2000)013<1517:PEATHD>2.0.CO;2.

Wang, B., J. Yang, T. J. Zhou, and B. Wang, 2008: Interdecadal changes in the major modes of Asian-Australian monsoon variability: Strengthening relationship with ENSO since the late 1970s. *J. Climate*, **21**, 1771–1789, https://doi.org/10.1175/2007JCLI1981.1.

Wang, B., B. Q. Xiang, and J. Y. Lee, 2013: Subtropical high predictability establishes a promising way for monsoon and tropical storm predictions. *Proceedings of the National Academy of Sciences of the United States of America*, **110**, 2718–2722, https://doi.org/10.1073/pnas.1214626110.

Wang, L., and J.-Y. Yu, 2018: A recent shift in the monsoon centers associated with the tropospheric biennial oscillation. *J. Climate*, **31**, 325–340, https://doi.org/10.1175/JCLI-D-17-0349.1.

Wang, L., J.-Y. Yu, and H. Paek, 2017: Enhanced biennial variability in the Pacific due to Atlantic capacitor effect. *Nature Communications*, **8**, 14887, https://doi.org/10.1038/ncomms14887.

Wu, B., T. Li, and T. J. Zhou, 2010: Relative contributions of the Indian Ocean and local SST anomalies to the maintenance of the Western North Pacific anomalous anticyclone during the El Niño decaying summer. *J. Climate*, **23**, 2974–2986, https://doi.org/10.1175/2010JCLI3300.1.

Wu, R. G., Z. Z. Hu, and B. P. Kirtman, 2003: Evolution of ENSO-related rainfall anomalies in East Asia. *J. Climate*, **16**, 3742–3758, https://doi.org/10.1175/1520-0442(2003)016<3742:EOERAI>2.0.CO;2.

Wu, Z. W., and L. L. Yu, 2016: Seasonal prediction of the East Asian summer monsoon with a partial-least square model. *Climate Dyn.*, **46**, 3067–3078, https://doi.org/10.1007/s00382-015-2753-4.

Wu, Z. W., B. Wang, J. P. Li, and F. F. Jin, 2009: An empirical seasonal prediction model of the east Asian summer monsoon using ENSO and NAO. *J. Geophys. Res.*, **114**, D18120, https://doi.org/10.1029/2009JD011733.

Xiang, B. Q., B. Wang, W. D. Yu, and S. B. Xu, 2013: How can anomalous western North Pacific Subtropical High intensify in late summer? *Geophys. Res. Lett.*, **40**, 2349–2354, https://doi.org/10.1002/grl.50431.

Xie, S.-P., K. M. Hu, J. Hafner, H. Tokinaga, Y. Du, G. Huang, and T. Sampe, 2009: Indian ocean capacitor effect on Indo-Western Pacific climate during the summer following El Niño. *J Climate*, **22**, 730–747, https://doi.org/10.1175/2008JCLI2544.1.

Xie, S.-P., Y. Du, G. Huang, X.-T. Zheng, H. Tokinaga, K. M.

Hu, and Q. Y. Liu, 2010: Decadal shift in El Niño influences on Indo-Western Pacific and East Asian climate in the 1970s. *J. Climate*, **23**, 3352–3368, https://doi.org/10.1175/2010JCLI3429.1.

Yang, J. L., Q. Y. Liu, S.-P. Xie, Z. Y. Liu, and L. X. Wu, 2007: Impact of the Indian Ocean SST basin mode on the Asian summer monsoon. *Geophys. Res. Lett.*, **34**, L02708, https://doi.org/10.1029/2006GL028571.

Ye, H., and R. Y. Lu, 2011: Subseasonal variation in ENSO-related East Asian rainfall anomalies during summer and its role in weakening the relationship between the ENSO and summer rainfall in Eastern China since the late 1970s. *J. Climate*, **24**, 2271–2284, https://doi.org/10.1175/2010JCLI3747.1.

Yu, J.-Y., P.-K. Kao, H. Paek, H.-H. Hsu, C.-W. Hung, M.-M. Lu, and S.-I. An, 2015: Linking emergence of the Central Pacific El Niño to the atlantic multidecadal oscillation. *J. Climate*, **28**, 651–662, https://doi.org/10.1175/JCLI-D-14-00347.1.

Zhang, R. H., A. Sumi, and M. Kimoto, 1996: Impact of El Niño on the East Asian monsoon: A diagnostic study of the '86/87 and '91/92 events. *J. Meteorol. Soc. Japan*, **74**, 49–62, https://doi.org/10.2151/jmsj1965.74.1_49.

Zhang, W. J., and Coauthors, 2016: Unraveling El Niño's impact on the East Asian Monsoon and Yangtze River summer flooding. *Geophys. Res. Lett.*, **43**, 11375–11382, https://doi.org/10.1002/2016GL071190.